Tunable high-resolution synthetic aperture radar imaging

Arnold D. Kim and Chrysoula Tsogka

Department of Applied Mathematics, University of California, Merced, 5200 North Lake Road, Merced, CA 95343, USA

Key Points:

- Low SNR measurements
- Tunable high-resolution imaging
- Modified Kirchhoff migration method

Corresponding author: Chrysoula Tsogka, ctsogka@ucmerced.edu

Abstract

We have recently introduced a modification of the multiple signal classification (MUSIC) method for synthetic aperture radar. This method depends on a tunable, user-defined parameter, ϵ, that allows for quantitative high-resolution imaging. It requires however, relative large single-to-noise ratios (SNR) to work effectively. Here, we first identify the fundamental mechanism in that method that produces high-resolution images. Then we introduce a modification to Kirchhoff Migration (KM) that uses the same mechanism to produces tunable, high-resolution images. This modified KM method can be applied to low SNR measurements. We show simulation results that demonstrate the features of this method.

1 Introduction

In synthetic aperture radar (SAR) a single transmitter/receiver on a platform is used to probe an imaging region of interest by emitting pulses and then record the subsequent echoes as the platform moves along a flight path. SAR imaging methods use these measurements to reconstruct images of targets in the imaging region of interest.

The traditional SAR image is formed by evaluating the data at each measurement location at the travel time that it takes for the waves to propagate from the platform location to a point in the imaging region on the ground and back. This imaging method is called Kirchhoff Migration (KM). The resolution of the image produced by KM has a range resolution that is $O(c/B)$ with c denoting the wave speed, and B denoting the system bandwidth, and a cross-range resolution that is $O(\lambda_0 L/a)$ with λ_0 denoting the central wavelength, L denoting the characteristic distance from the platform to the imaging region, and a denoting the length of the synthetic aperture (Cheney & Borden, 2009).

The authors have recently developed a modification to the multiple signal classification method (MUSIC) for SAR imaging (Kim & Tsogka, 2021). This method includes a user-defined parameter, which we call ϵ, that allows for tunable, high-resolution images. Using this method, we obtain a range resolution that is $O(\sqrt{\epsilon}(c/B)(L/R))$ with R denoting the range distance from the flight path to the center of the imaging region, and a cross-range resolution of $O(\sqrt{\epsilon}(c/B)(L/a))$. The key here is that the user-defined parameter ϵ can be made arbitrarily small which, in turn, allows for tunable high-resolution quantitative images. However, this method is limited to measurements with relatively high signal-to-noise ratios (SNRs). Otherwise, one cannot reliably separate signal from noise, which is a key step in this method. The quantitative recovery of reflectivity information suffers most when the SNR becomes too low, but image resolution also suffers.

In many practical applications, SAR data are very noisy (Doerry, 2006). For these problems, the modification to MUSIC will not be effective because the SNR is not sufficiently high. For this reason, we seek to develop a new method that retains the tunable high-resolution feature of this method, but can accommodate measurements with low SNR. To do this, we first re-evaluate the modification to MUSIC and identify the fundamental mechanism leading to tunable high-resolution. This mechanism involves a simple rational transformation. We form the same rational transformation of the normalized KM image and obtain a tunable high-resolution version of the KM method. This method requires no additional computations beyond those required for KM. The result of this modification is a method with a range resolution that is $O(\sqrt{\epsilon}c/B)$ and a cross-range resolution that is $O(\sqrt{\epsilon}\lambda_0 L/a)$.

The remainder of this paper is as follows. In Section 2 we give a brief description of synthetic aperture radar imaging, our assumptions, and define the measurements. In Section 3 we briefly review the recent modification to MUSIC and identify the fundamental mechanism allowing for tunable high-resolution imaging. Using the insight gained

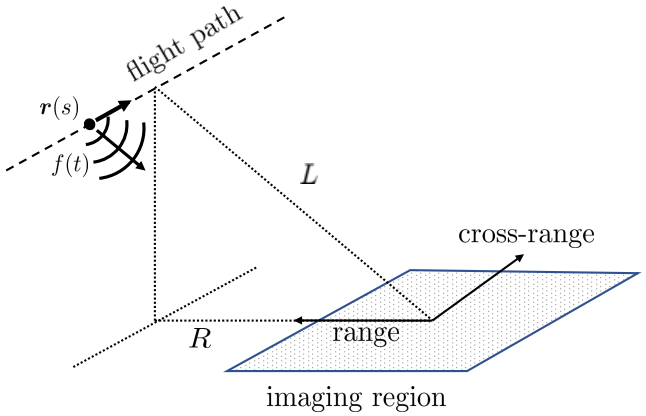

Figure 1. Setup for synthetic aperture radar imaging.

from identifying this fundamental mechanism, we introduce a modification to KM in Section 4. We show several simulation results in Section 5 that demonstrate the features of the modified KM method. Section 6 contains our conclusions.

2 Synthetic aperture radar imaging

We consider synthetic aperture radar (SAR) imaging in which a single transmitter/receiver on a moving platform emits and records signals (Cheney, 2001; Cheney & Borden, 2009; Moreira et al., 2013). A full set of measurements corresponds to a suite of experiments at several locations along the flight path. Let $f(t)$ denote the broadband pulse emitted and let $d(s,t)$ denote the data recorded which depends on the slow time s parameterizing the flight path of the platform, $\boldsymbol{r}(s)$, and the fast time t corresponding to the round-trip travel time between the platform and the imaging scene. Here, we assume the start-stop approximation in which the change in displacement between the targets and the platform is negligibly small compared to the travel time it takes for the pulse emitted to propagate to the imaging scene and return as echoes.

Figure 1 shows an illustration of SAR imaging. Here, we see that range is the coordinate obtained by projecting the vector that connects the center of the imaging region to the central platform location onto the imaging plane, and cross-range is the coordinate orthogonal to range. Denoting the size of the synthetic aperture by a and the system bandwidth by B, the typical resolution of the imaging system is $O((c/B)(L/R))$ in range and $O(\lambda L/a)$ in cross-range. Here c is the speed of light and λ the wavelength corresponding to the central frequency while L denotes the distance between the platform and the imaging region and R the offset in range.

With the start-stop approximation, measurements are taken at N discrete values of s, corresponding to $d(s_n,t)$ for $n=1,\cdots,N$. Next, we compute the discrete Fourier transform of digitally sampled values of $d(s_n,t)$ in t denoted by $d_n(\omega_m)$ for $m=1,\cdots,2M-1$. The full set of measurements is the $2M-1\times N$ matrix D whose columns are

$$\mathbf{d}_n = \begin{bmatrix} d_n(\omega_1) \\ d_n(\omega_2) \\ \vdots \\ d_n(\omega_{2M-1}) \end{bmatrix}, \quad n=1,\cdots,N. \tag{1}$$

The objective in SAR imaging is to identify and locate targets in an imaging region using these data.

3 MUSIC for SAR

The authors have recently extended MUSIC for SAR resulting in a tunable, quantitative high-resolution imaging method (Kim & Tsogka, 2021). The main limitation of this method is that it requires sufficiently high SNR to distinguish between signal and noise subspaces. We review this method here and identify the key mechanism that leads to tunable high-resolution images.

The key to applying MUSIC to SAR is a reorganization of the data matrix D which we explain below. Consider the nth column of D given in (1). Applying the Prony method (Prony, 1795) to this vector of length $2M-1$ yields the following $M \times M$ matrix,

$$D_n = \begin{bmatrix} d_n(\omega_1) & d_n(\omega_2) & \cdots & d_n(\omega_M) \\ d_n(\omega_2) & d_n(\omega_3) & \cdots & d_n(\omega_{M+1}) \\ \vdots & \vdots & \ddots & \vdots \\ d_n(\omega_M) & d_n(\omega_{M+1}) & \cdots & d_n(\omega_{2M-1}) \end{bmatrix}. \tag{2}$$

In this rearrangement, the first column is the truncation of $\mathbf{d}_n$ to its first M entries. Subsequent columns are sequential upward shifts of $\mathbf{d}_n$ truncated to its first M entries.

When there is no measurement noise and the frequencies are sampled at a fixed rate, (2) can be factorized as a sum of outer products, each corresponding to an individual point target (Kim & Tsogka, 2021). Suppose there are K point targets in the imaging region located at positions $\boldsymbol{y}_k$ with reflectivities ρ_k for $k = 1, \cdots, K$. It follows that

$$D_n = \sum_{k=1}^{K} s_k^{(n)} \mathbf{u}_k^{(n)} \mathbf{v}_k^{(n)\,H}, \tag{3}$$

with $s_k^{(n)} = \rho_k/(4\pi|\boldsymbol{x}_n - \boldsymbol{y}_k|)^2$,

$$\mathbf{u}_k^{(n)} = \begin{bmatrix} e^{\mathrm{i}2\omega_1|\boldsymbol{x}_n-\boldsymbol{y}_k|/c} \\ e^{\mathrm{i}2\omega_2|\boldsymbol{x}_n-\boldsymbol{y}_k|/c} \\ \vdots \\ e^{\mathrm{i}2\omega_M|\boldsymbol{x}_n-\boldsymbol{y}_k|/c} \end{bmatrix}, \quad \text{and} \quad \mathbf{v}_k^{(n)} = \begin{bmatrix} 1 \\ e^{-\mathrm{i}2\Delta\omega|\boldsymbol{x}_n-\boldsymbol{y}_k|/c} \\ \vdots \\ e^{-\mathrm{i}2(M-1)\Delta\omega|\boldsymbol{x}_n-\boldsymbol{y}_k|/c} \end{bmatrix}. \tag{4}$$

Here, $\boldsymbol{x}_n$ denotes the platform location at the nth measurement, $\omega_m = \omega_1 + (m-1)\Delta\omega$ for $m = 1, \cdots, M$, and c denotes the wave speed.

Assuming that $K < M$, we find that the column space of D_n is given by

$$\mathscr{S} = \mathrm{span}\{\mathbf{u}_1^{(n)}, \cdots, \mathbf{u}_K^{(n)}\}, \tag{5}$$

which corresponds to the signal subspace. Upon computing the singular value decomposition $D_n = U\Sigma V^H$, we find that the first K columns of U give an orthonormal basis for $\mathscr{S}$. Let $\tilde{U}$ be the $M \times K$ matrix corresponding to the first K columns of U. The projection onto the signal subspace is then $P_{\text{signal}} = \tilde{U}\tilde{U}^H$. The noise subspace is the orthogonal complement to the signal subspace. The projection onto the noise subspace is $P_{\text{noise}} = I_M - \tilde{U}\tilde{U}^H$ with I_M denoting the $M \times M$ identity matrix.

Now suppose we wish to test if a search point $\boldsymbol{y}$ somewhere in the imaging region corresponds to a target. We introduce the illumination vector,

$$\mathbf{a}_n(\boldsymbol{y}) = \begin{bmatrix} e^{\mathrm{i}2\omega_1|\boldsymbol{x}_n-\boldsymbol{y}|/c} \\ e^{\mathrm{i}2\omega_2|\boldsymbol{x}_n-\boldsymbol{y}|/c} \\ \vdots \\ e^{\mathrm{i}2\omega_M|\boldsymbol{x}_n-\boldsymbol{y}|/c} \end{bmatrix}. \tag{6}$$

In traditional MUSIC we form an image by testing if this illumination vector lies in the noise subspace. For this case, we compute $\|P_{\text{noise}}\mathbf{a}_n(\boldsymbol{y})\|^2$ for $n = 1, \cdots, N$, and form an image by plotting

$$I(\boldsymbol{y}) = \left[\sum_{n=1}^{N} \|P_{\text{noise}}\mathbf{a}_n(\boldsymbol{y})\|^2\right]^{-1}. \tag{7}$$

The basic idea behind this formation of an image is that when $\boldsymbol{y}$ corresponds to a target location, the projection onto the noise subspace will be zero, so plotting the reciprocal will yield a singularity there.

In the recent modifications to MUSIC (González-Rodríguez et al., 2021; Kim & Tsogka, 2021), both P_{noise} and P_{signal} are used. The motivating idea in those methods is that P_{noise} is used to identify and locate targets and that P_{signal} is used to deliver quantitative information about the target. However, there is a more generally useful reason to include both projections. By considering both P_{noise} and P_{signal}, one can introduce a continuous weighting in terms of a user-defined parameter $\epsilon > 0$ according to

$$\begin{aligned} I_\epsilon(\boldsymbol{y}) &= \left[\sum_{n=1}^{N} \epsilon^{-1}\|P_{\text{noise}}\mathbf{a}_n(\boldsymbol{y})\|^2 + \|P_{\text{signal}}\mathbf{a}_n(\boldsymbol{y})\|^2\right]^{-1} \\ &= \epsilon\left[\sum_{n=1}^{N}\left(1-(1-\epsilon)\frac{\left|\tilde{U}^H\mathbf{a}_n(\boldsymbol{y})\right|^2}{\|\mathbf{a}_n(\boldsymbol{y})\|^2}\right)\|\mathbf{a}_n(\boldsymbol{y})\|^2\right]^{-1}, \end{aligned} \tag{8}$$

where we have resubstituted our expressions for P_{noise} and P_{signal} into (8).

For a single target located at $\boldsymbol{y}_0$, we have found in a neighborhood about $\boldsymbol{y}_0$ that

$$\frac{\left|\tilde{U}^H\mathbf{a}_n(\boldsymbol{y})\right|^2}{\|\mathbf{a}_n(\boldsymbol{y})\|^2} \approx 1-\beta^2|\boldsymbol{y}-\boldsymbol{y}_0|^2 \tag{9}$$

for some β (Kim & Tsogka, 2021). Consider the simple function $f(x) = 1-\beta^2x^2$. It assumes its maximum value of 1 on $x = 0$. It assumes its full-width/half-maximum (FWHM) on $\Delta x^* = \pm 1/(\sqrt{2}\beta)$. Now consider the function,

$$F_\epsilon(x) = \frac{\epsilon}{1-(1-\epsilon)f(x)}. \tag{10}$$

This function also assumes its maximum value of 1 on $x = 0$, but it assumes its FWHM on

$$\Delta x^* = \pm\frac{\sqrt{\epsilon}}{\beta\sqrt{1-\epsilon}} = \frac{\sqrt{\epsilon}}{\beta} + O(\epsilon^{3/2}), \quad \epsilon \to 0. \tag{11}$$

Thus for a function $f(x)$ with some FWHM, we can instead consider the function $F_\epsilon(x)$ given in (10) with the same FWHM, but scaled by $\sqrt{\epsilon}$. It is through this simple mechanism that we have determined that this generalization of MUSIC for SAR has a range resolution that is $O(\sqrt{\epsilon}(c/B)(L/R))$ and a cross-range resolution that is $O(\sqrt{\epsilon}(c/B)(L/a))$.

The key point is the factor of $\sqrt{\epsilon}$ since ϵ can be made arbitrarily small. This tunable resolution can be used advantageously when forming images of targets. For example, the value of ϵ can be varied by the user based on the resolution of the mesh used to sample the imaging region. Upon identifying subregions where an individual target is located, one can then change the value of ϵ to obtain a very high resolution image of the target on a finer mesh.

4 Modified Kirchhoff Migration

The traditional method for SAR imaging uses Kirchhoff Migration (KM). This imaging method is robust to measurement noise. In fact, it is not restricted like MUSIC to problems where the signal subspace can be reliably distinguished from the noise subspace. For that reason, KM is robust for problems with very low SNR. Here, we give a modification of KM based off of what we have done for MUSIC to yield a KM imaging method with tunable resolution.

Using the data defined in (1), we form the KM image through evaluation of

$$I^{\mathrm{KM}}(\boldsymbol{y}) = \sum_{n=1}^{N} \sum_{m=1}^{2M-1} d_n^*(\omega_m) e^{\mathrm{i}2\omega_m |\boldsymbol{x}_n - \boldsymbol{y}|/c}, \tag{12}$$

with $d_n^*(\omega_m)$ denoting the complex conjugate of $d_n(\omega_m)$. It is well known that the resolution of I^{KM} is $O(c/B)$ in range and $O(\lambda L/a)$ in cross-range.

The inner sum over frequencies in (12) is an inner product, so it can be interpreted as a projection of the illumination vector

$$\mathbf{a}_n(\boldsymbol{y}) = \left[e^{\mathrm{i}2\omega_1 |\boldsymbol{x}_n - \boldsymbol{y}|}, \cdots, e^{\mathrm{i}2\omega_{2M-1} |\boldsymbol{x}_n - \boldsymbol{y}|} \right]^T, \tag{13}$$

onto the data vector

$$\mathbf{d}_n = \left[d_n(\omega_1), \cdots, d_n(\omega_{2M-1}) \right]^T, \tag{14}$$

or

$$I^{\mathrm{KM}}(\boldsymbol{y}) = \sum_{n=1}^{N} \mathbf{d}_n^H \mathbf{a}_n(\boldsymbol{y}). \tag{15}$$

Let $\mathbf{d}_n = \hat{\mathbf{d}}_n \|\mathbf{d}_n\|$ and $\mathbf{a}_n(\boldsymbol{y}) = \hat{\mathbf{a}}_n(\boldsymbol{y}) \|\mathbf{a}_n(\boldsymbol{y})\|$. Just as we have done for MUSIC, we form a tunable KM imaging functional through evaluation of

$$I_\epsilon^{\mathrm{KM}}(\boldsymbol{y}) = \epsilon \left| \sum_{n=1}^{N} \left(1 - (1-\epsilon) \hat{\mathbf{d}}_n^H \hat{\mathbf{a}}_n(\boldsymbol{y}) \right) \right|^{-2}. \tag{16}$$

This modification of KM will yield an image with a tunable resolution that scales as $\sqrt{\epsilon}$. We expect that this imaging method will have a range resolution that is $O(\sqrt{\epsilon} c/B)$ and a cross-range resolution that is $O(\sqrt{\epsilon}\lambda_0 L/a)$. Since ϵ is a user-defined parameter, it can be made arbitrarily small to produce a very high-resolution image.

The mechanism through which (16) achieves high resolution requires that $\hat{\mathbf{d}}_n^H \hat{\mathbf{a}}_n(\boldsymbol{y}) = 1$ on target locations. When considering an imaging region with multiple targets, this requirement may not be met exactly on all target locations. Therefore, (16) may not clearly identify some of the targets. However, if (16) is used in a sub-region containing a single target, it will produce tunable high-resolution images of that individual target.

5 Numerical results

We use numerical simulations to test and evaluate the imaging method presented above. We used the following values for the system parameters which are based on the

GOTCHA data set (Casteel Jr et al., 2007). We set the origin of a coordinate system in the middle of a 4.8 m × 4.8 m imaging region situated at ground level, $z = 0$. The x-coordinate is cross-range and the y-coordinate is range. The coordinates along the linear flight path where measurements are taken are $\boldsymbol{x}_n = (x_n, R, H)$ with $x_n = -a/2 + a(n-1)/(N-1)$ for $n = 1, \cdots, N$. Here, the range of the flight path is $R = 7.10$ km and the height is $H = 7.30$ km, so that $L = \sqrt{H^2 + R^2} = 10.18$ km. The length of the synthetic aperture is $a = 0.13$ km. The central frequency is $f_0 = 9.6$ GHz and the bandwidth is $B = 622$ MHz. Using $c = 3 \times 10^8$ m/s, we find that the central wavelength is $\lambda_0 = 3.12$ cm. We use $M = 31$ equi-spaced frequencies over the bandwidth and $N = 124$ spatial measurements.

5.1 Single target

We first apply the imaging method to a single point target located at $\boldsymbol{y}_0 = (1\,\text{m}, 1\,\text{m}, 0)$. We added measurement noise to the measured signal so that SNR = 15.3989 dB. The image resulting from applying KM given in (12) appears in the left plot and the image resulting from applying the modified KM given in (16) appears in the right plot of Fig. 2. For both plots, the image was normalized by its peak value and plotted in dB ($10\log_{10}$-scale). Additionally, the images are centered about the true target location.

Using the parameter values for this problem, we find that $c/B \approx 15\,\lambda_0$ and $\lambda_0 L/a \approx 79\lambda_0$ corresponding to the range (x) and cross-range (y) resolutions, respectively. The left plot shows a peak at the target location whose full-width/half-maximum (FWHM) corresponds to those resolutions estimates. Additionally, we see the familiar side-lobes that appear in KM images.

To form the image appearing the right plot of Fig. 2, we have used $\epsilon = 10^{-4}$ in the modified KM image. This image has a sharper peak at the target location with no apparent side-lobes. It has a much higher resolution than the KM image with less artifacts.

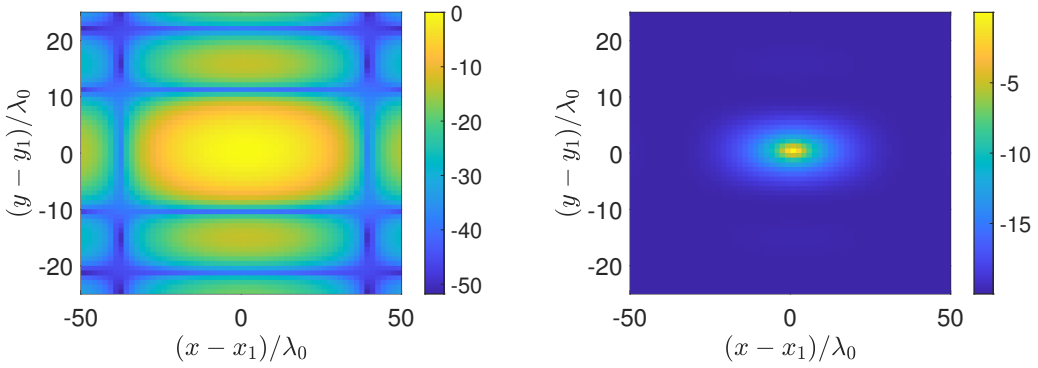

Figure 2. (Left) Image formed by KM centered on the target location, normalized by its peak value and plotted in dB ($10\log_{10}$-scale) with SNR = 15.3989 dB. (Right) Image formed using modified KM with $\epsilon = 10^{-4}$ for the same measurement data.

We expect that the image resolution of modified KM to be $O(\sqrt{\epsilon}c/B)$ in range and $O(\sqrt{\epsilon}\lambda_0 L/a)$ in cross-range. Using numerical simulations, we estimate the FWHM in range and cross-range for noiseless data for the same single target. The image resolution results are shown in Fig. 3. The plots in Fig. 3 show the computed FHWM in range ($\Delta x^*/\lambda_0$) as blue circles, and in cross-range ($\Delta y^*/\lambda_0$) as red squares. The left plot in Fig. 3 shows the FWHM results as a function of ϵ with c/B and $\lambda_0 L/a$ fixed. The center plot shows

FWHM results as a function of c/B with $\epsilon = 10^{-4}$ and $\lambda_0 L/a$ fixed. The right plot shows FWHM results as a function of $\lambda_0 L/a$ with $\epsilon = 10^{-4}$ and c/B fixed. All three of these plots show linear fits to the data as solid curves. The black dashed curve shows the expected behavior of the image resolution. These results verify the resolution estimates for modified KM.

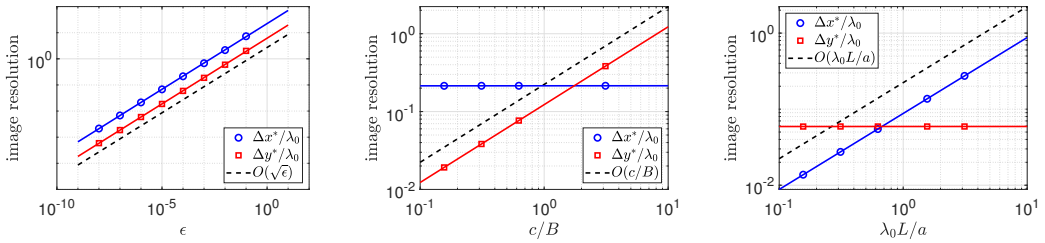

Figure 3. Computed full-width/half-maximum (FWHM) values of images produced with modified KM as a function of ϵ (left), c/B (center), and $\lambda_0 L/a$ (right).

5.2 Multiple targets

We now consider an imaging scene with three identical targets. The targets are located at $\boldsymbol{y}_1 = (-1.4\,\mathrm{m}, -0.5\,\mathrm{m}, 0\,\mathrm{m})$, $\boldsymbol{y}_2 = (-0.6\,\mathrm{m}, -1.2\,\mathrm{m}, 0\,\mathrm{m})$, and $\boldsymbol{y}_3 = (1.2\,\mathrm{m}, 1.1\,\mathrm{m}, 0\,\mathrm{m})$. The image formed using KM is shown in the left plot and the imaged formed using modified KM is shown in the right plot of Fig. 4. Measurement noise was added to the signals so that SNR $=$ 14.1217 dB. The KM image shows peaks at the target locations indicated as red "+" symbols. However, the interactions of the side-lobes yields several imaging artifacts. In contrast, the modified KM image is free from imaging artifacts and identifies sharp regions where the targets are located.

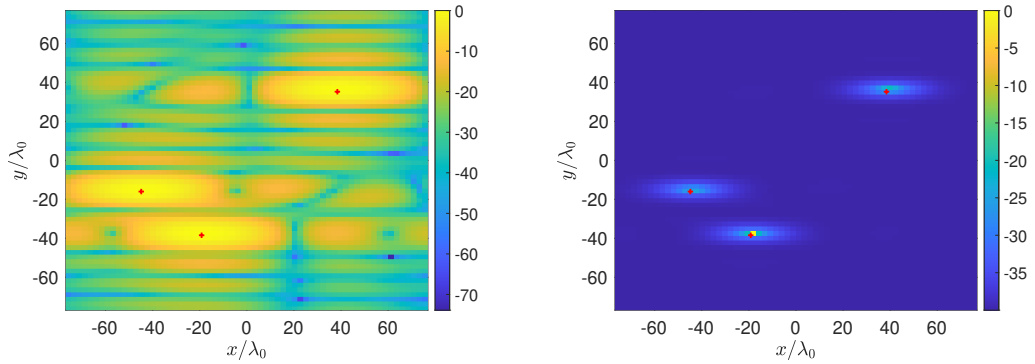

Figure 4. (Left) Image formed by KM normalized by its peak value and plotted in dB ($10\log_{10}$-scale) with SNR $=$ 14.1217 dB. (Right) Image formed using modified KM with $\epsilon = 10^{-4}$ for the same measurement data.

A challenge in using the modified KM is that it relies on an exact cancellation at a peak value that is normalized to one. When there are multiple targets and the KM image is normalized by its maximum value, presumably on only one of those targets incurs this exact cancellation. Consequently, the image of the other targets may not be as sharp. However, using the image shown on the right plot of Fig. 4, one can identify small sub-

regions where each of the three targets are located. If we were to evaluate the modified KM in each of these sub-regions, we expect to obtain high-resolution images of the individual targets because each of those images would be normalized by the maximum value in the small sub-region corresponding to the individual target.

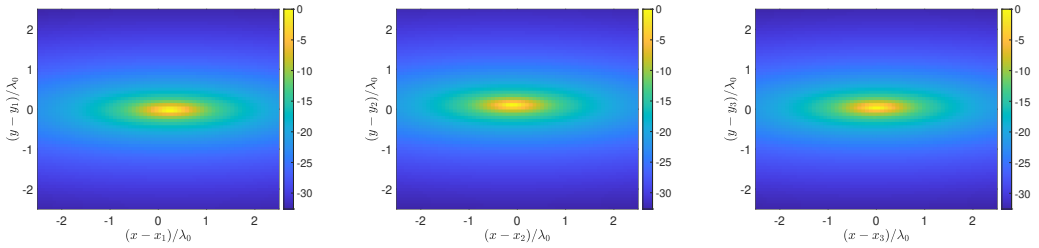

Figure 5. Close-up images of target 1 (left), target 2 (center), and target 3(center) in a small $5\lambda_0 \times 5\lambda_0$ sub-region about the target location using the same data used in Fig. 4. Each image is centered about the true target location and normalized by its maximum value.

In Fig. 5 we plot close-up images in a $5\lambda_0 \times 5\lambda_0$ sub-region centered about the true location of target 1 (left), target 2 (center), and target 3 (right) using $\epsilon = 10^{-4}$. The images are formed using the same data used in Fig. 4. The only difference is evaluating the modified KM only in a small sub-region. These images demonstrate the very high resolution achievable using modified KM. Moreover, the resolution achieved by this method is set by the user-defined parameter ϵ.

The results in Fig. 5 show that the images are not peaked at the exact target locations. They are misaligned by fractions of a wavelength. Because modified KM yields such high-resolution images of targets compared with KM, we find that it shows how noise affects KM, and hence modified KM. The images produced by KM and modified KM when we increase the noise such that SNR $= 4.1217\,\mathrm{dB}$ are shown in Fig. 6. The relative performance of both of these imaging methods appears to be the same as for the higher SNR case shown in Fig. 4. However, the plots of close-up images about each of the target locations shown in Fig. 7 using the high-resolution modified KM images show that the peaks are farther away from the true target locations than for the higher SNR case shown in Fig. 5, on the order of a wavelength. We see that this effect is more pronounced in cross-range than in range.

With very low SNR, the noise affects the phase of the measured signals in the form of random phase rotations. These phase rotations shift the predicted location of targets slightly. When plotting images using KM, the image resolution is too coarse to be able to observe these shifts in target locations. However, with modified KM, the resolution is so high that one observes these shifts. Our simulation results suggest that this random shifts in the target locations are bounded by a wavelength or less.

6 Conclusions

We have identified the fundamental mechanism leading to tunable high-resolution images with our generalization of MUSIC. Using that same mechanism we have introduced a simple modification to KM. This modification is a rational transformation of the normalized KM image that includes a user-defined parameter, which we call ϵ, that effectively tunes the resolution. We have shown that the resolution of the modified KM method is $O(\sqrt{\epsilon}c/B)$ in range and $O(\sqrt{\epsilon}\lambda_0 L/a)$ in cross-range. Because this user-defined parameter can be made arbitrarily small, we can achieve sub-wavelength resolution of

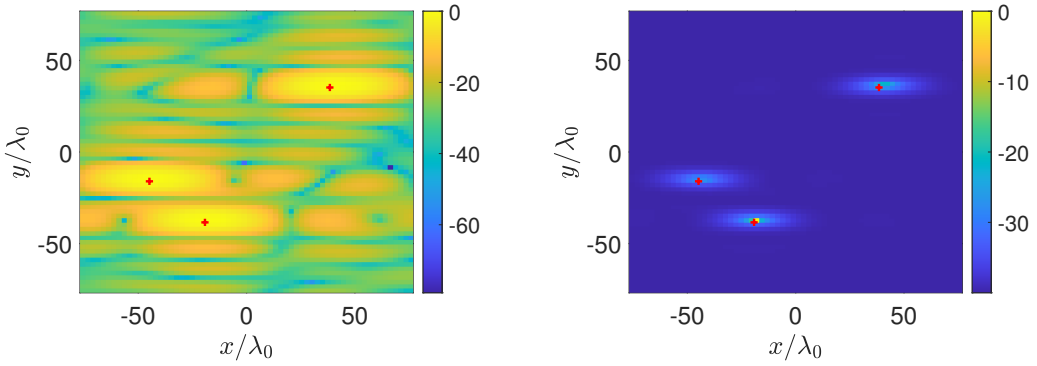

Figure 6. (Left) Image formed by KM normalized by its peak value and plotted in dB ($10\log_{10}$-scale) with SNR $= 4.1217\,\text{dB}$. (Right) Image formed using modified KM with $\epsilon = 10^{-4}$ for the same measurement data.

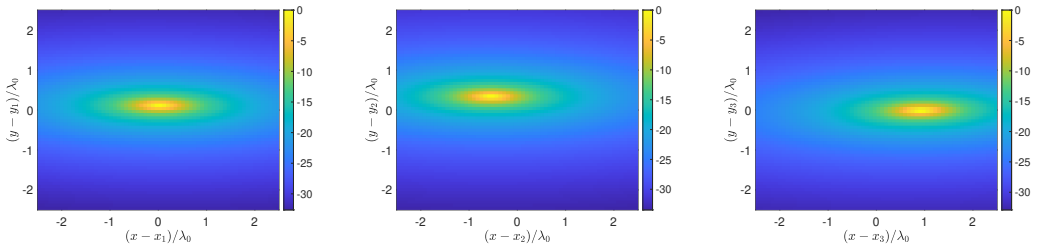

Figure 7. Close-up images of target 1 (left), target 2 (center), and target 3(center) in a small $5\lambda_0 \times 5\lambda_0$ sub-region about the target location with SNR $= 4.1217\,\text{dB}$.

targets using this method. In contrast to MUSIC, this modified KM method can be applied to measurements with low SNR.

When SNR is very low, the modified KM image of targets is shifted from their true location. We are able to observe these shifts because the modified KM produces such high resolution images. These shifts in the target locations are due to noise causing phase perturbations to measurements. In our simulations, we have observed that when SNR $\approx$ 0 dB, these shifts are on the order of a wavelength.

Because this modified KM method can be applied with no additional cost beyond the KM method, itself, and because it produces tunable, high-resolution images, we believe that this method is very useful for a broad variety of SAR imaging problems.

Acknowledgments

The authors acknowledge support by the Air Force Office of Scientific Research (FA9550-21-1-0196). A. D. Kim also acknowledges support by the National Science Foundation (DMS-1840265).

References

Casteel Jr, C. H., Gorham, L. A., Minardi, M. J., Scarborough, S. M., Naidu, K. D., & Majumder, U. K. (2007). A challenge problem for 2d/3d imaging of targets from a volumetric data set in an urban environment. In *Algorithms for synthetic aperture radar imagery xiv* (Vol. 6568, p. 65680D).

Cheney, M. (2001). A mathematical tutorial on synthetic aperture radar. *SIAM Review*, *43*(2), 301–312.

Cheney, M., & Borden, B. (2009). *Fundamentals of Radar Imaging* (Vol. 79). SIAM.

Doerry, A. W. (2006). *Performance limits for synthetic aperture radar – second edition* (Tech. Rep. No. SAND2006-0821). Sandia National Laboratories.

González-Rodríguez, P., Kim, A. D., & Tsogka, C. (2021). Quantitative signal subspace imaging. *Inverse Probl.*. doi: 10.1088/1361-6420/ac349b

Kim, A. D., & Tsogka, C. (2021). *High-resolution, quantitative signal subspace imaging for synthetic aperture radar.*

Moreira, A., Prats-Iraola, P., Younis, M., Krieger, G., Hajnsek, I., & Papathanassiou, K. P. (2013). A tutorial on synthetic aperture radar. *IEEE Geosci. Remote Sens. Mag.*, *1*(1), 6–43.

Prony, G. R. B. (1795). Essai experimental et analytique sur les lois de la dilatalrlite de fluids elastiques et sur cells de la vapeur de l'alcool, à différents tempoeratures. *J. de l'Ecole Polytech.*, *1*, 24–76.